Measurement 222 (2023) 113655



Contents lists available at ScienceDirect

Measurement

journal homepage: www.elsevier.com/locate/measurement



Prediction of thrust force in indexable drilling of aluminum alloys with machine learning algorithms

Aslan Akdulum [a,*], Yunus Kayir [b]

[a] Department of Machinery and Metal Technologies, Başkent OSB Vocational School of Technical Sciences, Hacettepe University, Ankara, Turkey
[b] Faculty of Technology, Department of Manufacturing Engineering, Gazi University, Ankara, Turkey

ARTICLE INFO

Keywords:
Thrust force
Hybrid modeling
Machine learning
Pearson correlation sorting
Prediction

ABSTRACT

The thrust force has a direct effect on important output responses such as surface roughness, power consumption, and tool wear. The measurement process for thrust forces is very time-consuming and costly. Low success rates are achieved in the estimation of thrust force. The mechanical properties and chemical composition of the workpiece material were not taken into account as input properties in the previously established models. However, these features are of high importance in the formation of the thrust force. In this study, it is aimed at estimating the thrust force with the least input feature with a high success rate by establishing single and hybrid models with different machine learning algorithms. As a result, the thrust force can be successfully predicted by machine learning algorithms by entering two properties. Successful thrust force estimation will provide more accurate process planning, material selection, and optimization.

1. Introduction

Aluminum is the third-most prevalent metal on earth. Its alloys are used extensively and increasingly in automotive, aerospace, defense, and various other industries [1]. For example, while 180 kg of aluminum is used per vehicle in the automotive field today, it is estimated that this rate will increase by 70% until 2025 [2]. Alloys with different chemical compositions are produced to increase the durability of the aluminum or to add properties [3]. Especially within the aviation industry, 2xxx, 6xxx, and 7xxx series aluminum alloys have been increasingly preferred since the 1930s [4]. The common feature of these alloys is that they are heat treatable; in other words, they are aging. Due to their favorable replacement of cast iron and steel in the production of parts and versatility, these alloys are consequently responsible for the majority of machining operations in the aerospace and automotive industries [5]. It is expected that the application of these alloys in many industries would rise over time. Machining operations such as milling, turning, or drilling are applied as a final process to shape aluminum alloys according to the usage area.

Among these operations, the drilling process alone accounts for more than one-third of the total metal cutting operations [6]. For drilling holes, cutting tools called drills with various features are used. Drills can be produced from one material, or the body and cutting insert can be made of different materials. Indexable insert drills, or U drills, are used especially for drilling large-diameter holes [7]. The body and cutting insert of U drills are produced from different materials. The cutting inserts can have different properties in terms of geometry, coating, and chip-breaker form based on the material being processed. The market share of U drills is around 8% in the total cutting tool market and around 53% in drilling tools [8]. However, when the literature is examined, there are not enough studies about it. Its features are not fully understood, and development studies are carried out in both the academic and production sectors. One of these research and development areas is the thrust force that occurs in drilling with U drills.

The thrust force is one of the most crucial hole quality parameters to make sense of hole-making operations. The thrust force generated during drilling has a high impact on output parameters such as tool wear, temperature, power consumption, vibration, surface roughness, chip morphology, and dimensional accuracy [9]. Generally, the thrust force is investigated by establishing relationships according to its response to various input parameters, including feed rate and cutting speed. Generally, three-component force measurement dynamometers are used to measure thrust force. For measuring operations, the dynamometer is difficult to set up because extra clamping tools are needed. Costly and not suitable for use in a real production environment [10]. Although real-time recording is possible, offline data processing is required to use

* Corresponding author.
E-mail addresses: a.akdulum@gmail.com (A. Akdulum), ykayir@gazi.edu.tr (Y. Kayir).

https://doi.org/10.1016/j.measurement.2023.113655
Received 3 August 2023; Received in revised form 22 September 2023; Accepted 1 October 2023
Available online 2 October 2023
0263-2241/© 2023 Elsevier Ltd. All rights reserved.

this data. For each different material, these measurements and relationships need to be established based on experiments. Since the measurement of all parts is difficult and not efficient, alternative methods are being investigated [11]. Modeling and estimation of thrust force according to cutting tool, drilling parameters, and workpiece material is a current research topic. Because successful thrust force estimation is very important for process planning, material selection, and optimization.

High success rates have been achieved in modeling and estimating thrust force for normal twist drills [12]. However, because the two cutting inserts in U drills are at various distances and angles from the hole axis, the central insert's penetration effect causes failure in modeling and estimation of the thrust force [13]. Therefore, alternative methods continue to be tried. Some methods have been tried in the studies carried out so far. The thrust force for U drills was examined by finite element analysis (FEA) according to the input parameters, and it was determined that the insert in the center was responsible for the higher thrust force [14]. Experimental results compared with FEA for dry and cryogenic environments [15]. In dry conditions, the thrust force was approximately 3% higher in the experimental results, while it was approximately 3% lower in cryogenic conditions. They attributed this to the friction-reducing effect of cryogenic conditions. In a very detailed study comparing FEA and experimental results, it was determined that approximately 55% of the thrust force was generated by the central insert [16]. In addition, in the same study, an estimation error between 12% and 20% occurred in the thrust force modeled with FEA, according to the feed rate. It has been stated that this prediction error is caused by different friction mechanisms at the central and peripheral inserts. In another study, the inserts were mathematically modeled and compared with experimental results [17]. However, in order to get rid of the central insert's penetrating effect, pre-drilling tests were carried out, and a successful estimation result was obtained as a result. In another study by the same authors, an estimation was made between the mathematical result and the experimental result with an error of 60% [13]. In this study, they attributed this high error value to the penetrating effect of the central insert of the U drill since the front hole was not drilled. In another study, regression analysis was performed for the thrust force according to the input parameters, and as a result, the equations were found [7]. The equations found explained the model at a rate of 97.5%. Another study modeled cutting forces using a mechanistic approach [18]. The cutting force coefficients required for the method were determined with the data obtained from the real experimental processes for both central and peripheral inserts, and it was determined that the experimental and simulation results were compatible. In this study, the modeling of thrust force was investigated using Artificial neural networks (ANN), Taguchi, and Adaptive neuro-fuzzy inference systems (ANFIS) methods. Experimental data was directly used for making predictions, resulting in MAPE values of 5.07%, 0.57%, and 2.4% for the Taguchi, ANN, and ANFIS, respectively. However, when estimations were made based on SN ratios, the corresponding values were calculated as 0.84%, 0.18%, and 2.46% [19]. When the studies in the literature on modeling and estimation of thrust force for U drills are examined, modeling and estimation studies have been carried out with FEA, mathematical, mechanistic, Taguchi, ANN, and ANFIS methods. When the studies are examined, the number is quite low, and there is information that needs confirmation. This issue needs to be clarified with further studies. In certain studies, it has been indicated that the suboptimal predictions of thrust force can be attributed to the variation in the distances, angles, and geometric characteristics of the cutting inserts of U drills on the workpiece [20]. There is no point angle and no chisel edge as in normal twist drills [21]. In U drills, the presence of two cutting inserts, with one positioned at the center and the other at the periphery, induces imbalanced radial forces, leading to the occurrence of distinct cutting mechanisms at each insert [22]. The disparate cutting behavior arises from the fact that one of the cutting inserts performs machining at the center of the hole, while the other engages in cutting along the hole wall and its vicinity. The rise in cutting speed from the hole center to the hole wall causes different cutting mechanics to occur at each insert [23]. In addition, for FEA, mathematical modeling, and mechanistic modeling, it is necessary to calculate separately for each insert, and the required computation time is quite high. Repeating these processes for each cutter and material requires very high labor power. Considering the resulting success rates, there is a need for methods that exhibit a cost-effective propulsion modeling and estimation approach in terms of both time and labor. Stable and generalized results can be obtained with the methods to be developed. Therefore, there is merit in developing or exploring novel modeling and prediction methods to address this issue.

Among these new methods, artificial intelligence supported prediction models have very high success rates and have gained popularity recently. Artificial intelligence is a field where machine learning algorithms can make very high-level predictions with low computation time and high modeling capability. Machine learning algorithms are successfully applied in many different fields. With machine learning algorithms, models can be made to solve various problems such as classification, regression, and clustering. Regression algorithms are used in the estimation of numerical data such as thrust force. It has been used to predict various outputs for the machinery and manufacturing sectors in previous studies in the literature. In a study, the thrust force used to drill composite laminates using standard helical drills was very successfully predicted and modeled using the gaussian process regression (GPR) machine learning technique [24]. The estimation of cutting forces in turning operations was applied with high accuracy by support vector machines (SVM), GPR, and ANN methods [25]. Residual properties occurring in the whirling milling process were estimated by neural networks and the SVM method [26]. Surface residual stress occurring in the end milling was examined by the GPR method [27]. Modeling using the XGBoost and ANN approaches was used to examine how input variables affected the strength of CFRP materials [28]. While factors like depth of cut, feed rate, and cutting speed are typically taken into account in these modeling processes as input parameters, the chemical or mechanical characteristics of the material used for the workpiece are only used to explain how input parameters affect output parameters. However, the chemical composition and mechanical properties have a great influence on the output responses that result from machining a material. For example, in aluminum alloys, the thrust force and therefore the hole's quality are directly influenced by chips sticking to the hole wall and the built-up edge (BUE) on the cutting edge [29]. For example, the copper (Cu) element creates $CuAl_2$ compounds in the aluminum material, increasing the hardness of the alloy, making the chips that become brittle break faster, reducing the tendency to stick to the cutter and the machining surface, and improving the machinability [30]. As the copper ratio increases, the thrust force decreases [5]. The major alloying element in aging (precipitation hardening) aluminum alloys is Cu for 2xxx series alloys, Mg-Si for 6xxx series alloys, and Mg-Zn for 7xxx series alloys. In these alloys, different secondary phases occur in the microstructure due to the difference in element ratios and the applied heat treatments. Therefore, the mechanical properties of each alloy are unique. The microstructure and, subsequently, mechanical characteristics are altered by each chemical component and aging process [31]. Due to the aforementioned circumstances, while creating a prediction model using machine learning techniques, in addition to input variables like cutting speed and cutter, it is possible to take into account the chemical and mechanical characteristics of the materials used in the workpiece. Thus, thrust force can be estimated for a given material class by entering its chemical composition and mechanical properties. For example, it is thought that with the data obtained from 2xxx, 6xxx, and 7xxx series alloys in the aluminum class, thrust force estimation can be made for more specific 2024-T351 alloys or different alloys. The chemical and mechanical characteristics of a material can be easily learned from the certificate issued by the manufacturer, and the desired information can be found by using different material databases. With the help of the model established by the proposed method, the thrust forces

of any alloy belonging to a material class can be estimated. It is a desirable goal to achieve high forecasting success with the least input data. In order to achieve this, the output responses were estimated with the help of feature selection and ranking algorithms with high correlation and minimum input parameters in various studies [32]. For this purpose, the features were listed with the Pearson correlation method for the estimation of the output responses with the fewest input parameters [33]. By adding one feature at a time, a dataset was created

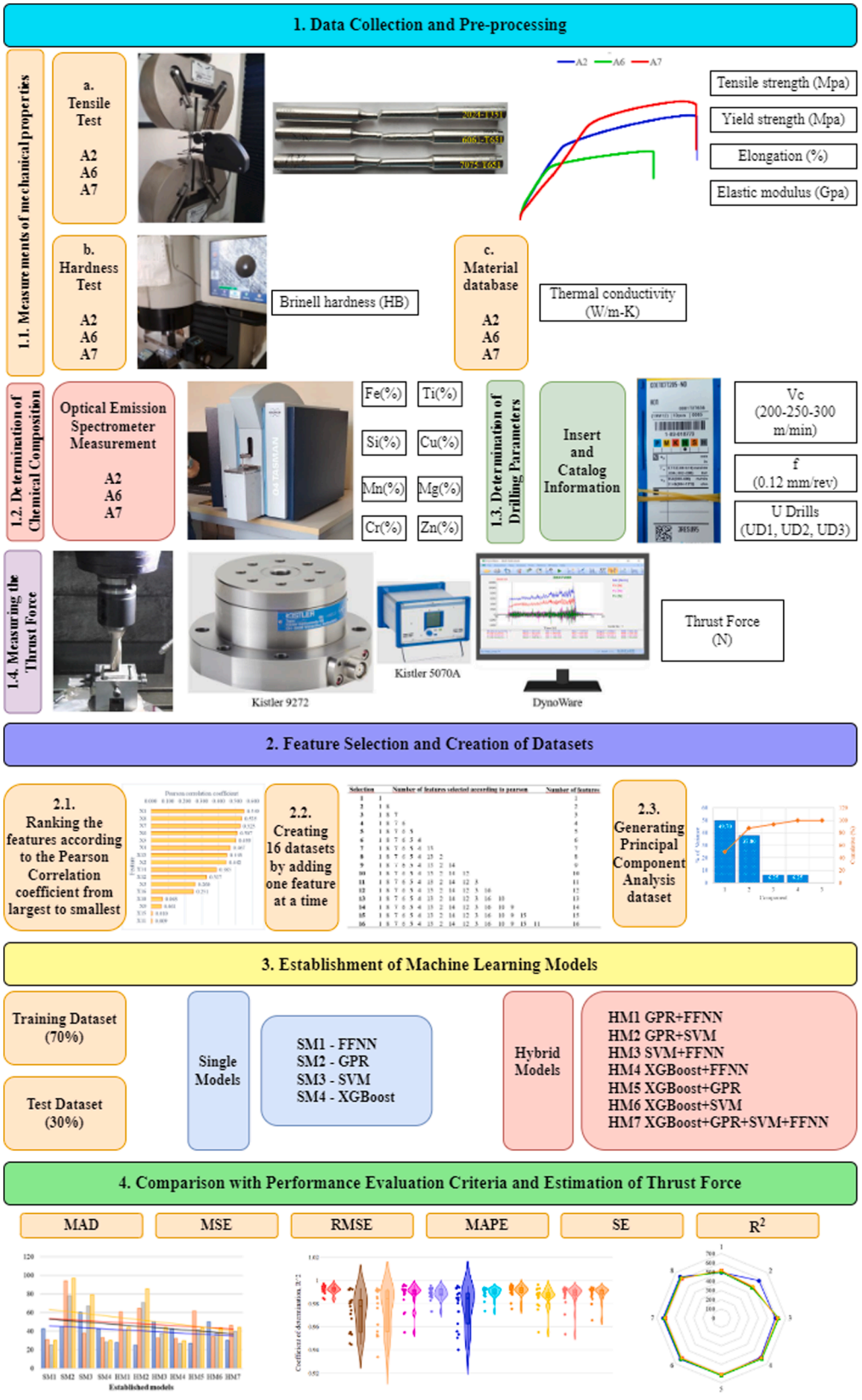


Fig. 1. General methodology for estimating thrust force with minimal input data.

as large as the number of features. Machine learning methods were used to generate the prediction models for each dataset. The estimated success of the generated models was calculated and evaluated using several assessment criteria.

In this study, it is aimed to estimate the thrust force in the indexable drilling of aluminum alloys with U drills with machine learning algorithms by entering the minimum number of chemical composition, mechanical properties, and cutting parameters. Popular machine learning techniques like SVM, GPR, multilayer feedforward neural networks (FFNN), and XGBoost are also utilized for this, along with hybrid structures created by mixing the aforementioned algorithms. Performance evaluation criteria were calculated using the data obtained with the help of all the established models and compared with each other. The distinctive contribution of this study is the precise prediction of the thrust force during indexable drilling of aluminum alloys utilizing U drills, as well as the building of models using machine learning approaches that take into consideration chemical composition and mechanical properties.

2. Material and method

This study was created using the general methodology shown in Fig. 1.

2.1. Machine learning

There are some important factors to consider when choosing appropriate machine learning algorithms for modeling purposes. Some of these important factors are the nature of the data, type of problem, amount of data, number of features, speed, transferability of data, overfitting, generalization ability, interpretability, hyperparameter tuning, performance of the model, etc. [34]. In this work, machine learning methods XGBoost, GPR, SVM, and FFNN were employed. The hybrid structures in Table 1 were created by employing the aforementioned techniques, and each technique was employed as a standalone prediction model. Because of their excellent rate of precision and brief learning requirements, these methods have been favored. Many different studies in the literature use these techniques. Both the values of the input features and the thrust values consist of quantitative data. Therefore, the estimation of the thrust force was made with regression algorithms.

Single machine learning models have been used to build hybrid models. Hybrid models are established by averaging the estimation results of two single methods. For example, if the output response was calculated as 2 by the GPR method and as 4 by the SVM method, the output response value of the hybrid GPR + SVM method was accepted as $(2 + 4)/2 = 3$. The evaluation of performance criteria were derived separately for each approach after processing all the data using the selected models. In machine learning, the training set and test set are two essential datasets used to develop and evaluate a machine learning model. These datasets play distinct roles in the model development and validation processes. To use machine learning methods, 27 pieces of data are divided in two. Thirty percent of the data (8 data) were utilized for testing, and seventy percent (19 data) were used for training. The machine learning methods used to model each dataset were trained on the same data, and then tested on the same data. Missing or corrupted data in datasets can be a major problem when building a machine learning model. Therefore, all of the input properties determined in all data sets were checked. For successful estimation of thrust force, features with full data were selected. Due to the high success rate of estimation in the literature, the FFNN method was used to obtain optimal training and test data. The number of neurons used to model the training and test data ranged from 1 to 100. Optimal training and test datasets were obtained by comparing the established models with the performance evaluation criteria. The determined training and test data were used to predict the thrust force with single and hybrid machine learning models.

Table 1
Single and hybrid machine learning.

Symbol	Single machine learning	Symbol	Hybrid machine learning
SM1	FFNN	HM1	GPR + FFNN
SM2	GPR	HM2	GPR + SVM
SM3	SVM	HM3	SVM + FFNN
SM4	XGBoost	HM4	XGBoost + FFNN
		HM5	XGBoost + GPR
		HM6	XGBoost + SVM
		HM7	XGBoost + GPR + SVM + FFNN

SM = Single model, HM = Hybrid model.

2.1.1. Extreme gradient boosting regression model

XGBoost was developed by Tianqi Chen and Carlos Guestrin [35]. The gradient boosting approach is implemented efficiently and effectively by the machine learning method known as XGBoost. Gradient boosting is an ensemble technique that generates several decision trees and combines their forecasts to increase the model's precision and generalizability. XGBoost has several advantages over other gradient boosting algorithms, such as preventing overfitting, increasing stability, processing large-scale datasets, and offering various features and hyperparameters. XGBoost is a powerful gradient boosting algorithm used to perform supervised machine learning tasks. This algorithm basically creates a series of decision trees. It starts with a single tree at the beginning and then improves the model by adding new trees at each iteration. At each iteration, new trees are created to correct the prediction errors of the existing model. It also uses regulatory terms to avoid overfitting. XGBoost provides importance scores that measure the contribution of each feature to the predictions, thus helping to understand the internal structures of the data. It also achieves fast results using parallel processing. Therefore, it is useful in various machine learning tasks with its high predictive accuracy and fast processing capability. To get better results with XGBoost, hyperparameters can be adjusted carefully, unnecessary or low-information features in the data set can be removed, more data can be added to the data set, and ensemble models can be established [36].

2.1.2. Gaussian process regression model

A nonparametric, probabilistic kernel-based technique called the GPR can forecast results and provide uncertainty bounds for regression issues [37]. A GPR model assumes that the data points were produced by a multivariate Gaussian process, which is composed of random factors. A GPR model can incorporate prior knowledge through the choice of kernel functions, which determine the covariance structure of the Gaussian process.

2.1.3. Support vector machine regression model

Both classification and regression issues can be solved using the supervised learning technique known as SVM [38]. It is predicated on the notion of locating a function that has a modest norm value, fits the data well, and is as flat as feasible. In order to handle nonlinear data and translate it into a space with greater dimensions where a linear function may be identified, SVM regression uses kernel functions.

2.1.4. Multilayer feedforward neural network model

An artificial neural network called an FFNN is made up of several layers of neurons connected by weighted links [32]. FFNN can learn complex nonlinear functions from input to output by adjusting the weights through a learning algorithm. FFNNs are widely used for various applications such as classification and regression.

''Levenberg-Marquardt'' is the learning algorithm used in this work. Each neuron's novel design was made by altering the number of neurons from 1 to 100. The study took advantage of the neuron structure that

performed the best.

2.1.5. Performance evaluation criteria

30% of the total dataset was used for testing, and the remaining 70% for training. The training dataset is prepared using machine learning techniques. Utilizing the unused test dataset, the generated model's performance was evaluated. The following performance evaluation metrics were used in this work to compare test datasets: mean absolute percentage error (MAPE), mean absolute difference (MAD), root mean square error (RMSE), standard error (SE), mean square error (MSE), and coefficient of determination (R^2). Multiple performance evaluation criteria were chosen to effectively compare the actual value of thrust force with the thrust force estimates made by the models. A small value is better for MAD, MSE, RMSE, MAPE, and SE values, while a R^2 value closest to 1 is better. Formulas for performance evaluation criteria are found in equations (1)–(6). n represents quantity of samples, t_i the actual values, y_i the estimated values, $\bar{t}_i$ the mean of the actual values.

$$MAPE = \frac{1}{n}\sum_{i=1}^{n}\frac{|t_i - y_i|}{t_i} \times 100 \quad (1)$$

$$MSE = \frac{1}{n}\sum_{i=1}^{n}(t_i - y_i)^2 \quad (2)$$

$$RMSE = \sqrt{\frac{1}{n}\sum_{i=1}^{n}(t_i - y_i)^2} \quad (3)$$

$$MAD = \frac{1}{n}\sum_{i=1}^{n}|t_i - y_i| \quad (4)$$

$$SE = \sqrt{\frac{\sum_{i=1}^{n}(t_i - y_i)^2}{n-2}} \quad (5)$$

$$R^2 = 1 - \frac{\sum_{i=1}^{n}(t_i - y_i)^2}{\sum_{i=1}^{n}(t_i - \bar{t}_i)^2} \quad (6)$$

2.2. Experimental setup

The experimental setup was conducted to estimate the thrust force generated in indexable drilling of aluminum alloys. As the U drill tries to penetrate the workpiece along the hole axis, as schematized in Fig. 2, a thrust force is applied to the U drill by the workpiece. In addition, the two inserts in the U drill are responsible for cutting different areas at the bottom of the hole. Therefore, the thrust force directly affects the hole quality.

For the experimental study, AA 2024-T351 (A2), AA 6061-T651 (A6), and AA 7075-T651 (A7) materials were prepared and used in 40 × 40 × 40 mm dimensions. Spectrum analysis was used to compare the chemical composition of the workpiece materials received with the certificate, and tensile testing and hardness measurements were used to compare the mechanical qualities. The material database is used to retrieve the workpiece materials' thermal conductivity data. The average of measurement data was calculated after at least three replications. Table 2 provides the chemical compositions of the workpiece materials as determined by the spectrum analysis. The calculated mechanical property values are shown in Table 3.

The drilling trials utilized both the through-hole and standard-hole drilling theories. The experiments were carried out utilizing a Johnford VMC-850 brand CNC vertical machining center. The operating system is Fanuc. The measurement accuracy is 1 μm.

The U drill is connected to the shaft using a tool holder of the Veldon type. The suggested drilling parameters were taken into consideration while producing the cutting tool catalog suggestions. Using the cutters' catalog information, cutting speed and feed rate numbers were calculated. In order to determine the feed rate constant (0.12 mm/rev), three different cutting speeds (200, 250, and 300 m/min) were used in the trials.

The experimental set-up shown in Fig. 3 was created to allow for real-time measurement of the thrust force produced when drilling aluminum alloys using a U drill. Thrust force was measured with a Kistler 9272 dynamometer, and an amplifier was employed with a Kistler 5070A. The accumulated signal information was processed with the dynoware program, which is the dynamometer's own software.

The nominal diameter of all U drills is 20 mm. The trials made use of

Table 2
% by weight chemical composition of the specified alloys.

	Fe	Si	Mn	Cr	Ti	Cu	Mg	Zn
A2	0.16	0.12	0.47	0.02	0.02	4.2	1.3	0.23
A6	0.5	0.68	0.15	0.17	0.027	0.32	0.98	0.16
A7	0.18	0.11	0.08	0.2	0.03	1.7	2.6	5.6

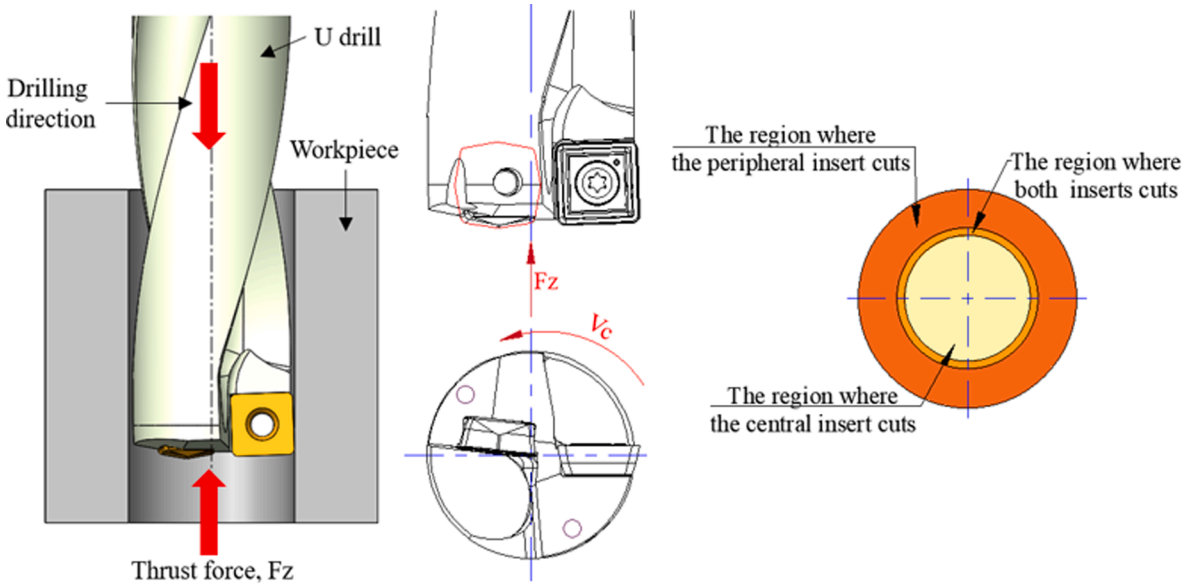


Fig. 2. Schematic representation of thrust force.

Table 3
Mechanical properties of the determined alloys.

	Tensile strength (Mpa)	Yield strength (Mpa)	Elongation (%)	Elastic modulus (Gpa)	Thermal conductivity (W/m-K)	Brinell hardness (HB)
A2	447.8	312.1	15.4	54.7	121	138
A6	253.1	278.1	9.1	62.1	167	115
A7	503.8	468.5	10.5	57	130	172

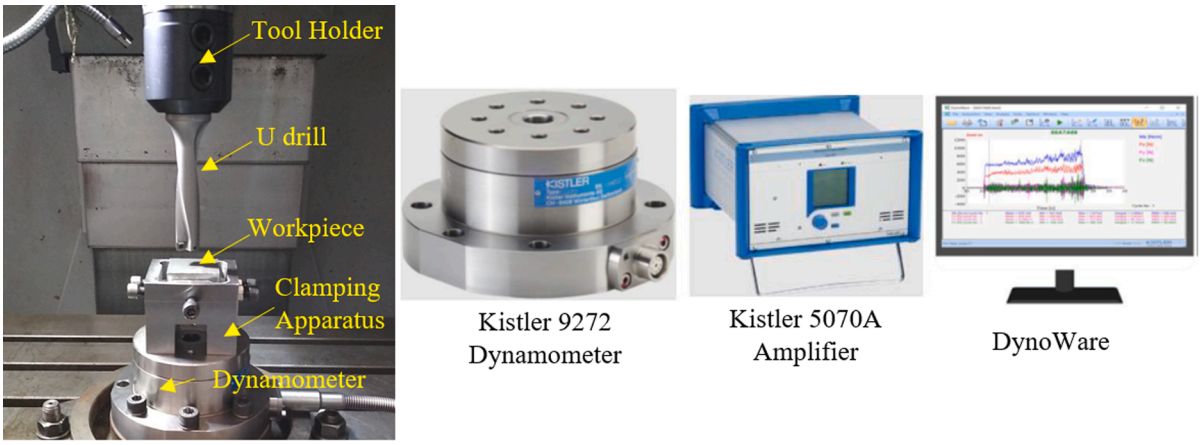


Fig. 3. Thrust force measurement experimental setup.

three different U drills. In Fig. 4, the size information of the used inserts is available. Table 4 provides the size details for the U drills used in the trials. In U drills, the central and peripheral inserts are typically used, however they differ slightly. Coating and edge geometry can change as a result of the various cutting speeds and load conditions they work under. Although the center and periphery inserts of the U drill in this study have different geometrical properties, both are uncoated tungsten carbide inserts that are suitable for cutting aluminum. The center insert was built of XOET 07 T205-ND, and the periphery inserts were formed of SPET 07 T208-ND geometry and *H*01 grade inserts. Use is made of U drills with similar inserts and the same nominal diameter.

Table 4
Comparing U drill sizes.

U Drills	Drill diameter, mm	Drill length, mm
UD1	20	60
UD2		80
UD3		100

2.3. Data collection

16 properties, including chemical composition, mechanical properties, and drilling parameters, were determined for machine learning models established by using thrust force values obtained as a result of indexable drilling of 27 aluminum workpieces. The determined features are given in Table 5. The purpose of determining these properties is to calculate the thrust force using the minimum input properties in the indexable drilling of aluminum materials. The experimental thrust force was determined by averaging the force signals received from the dynamometer in real time. The property numbers for X2, X3, and X16 are 2, 3, and 16, respectively.

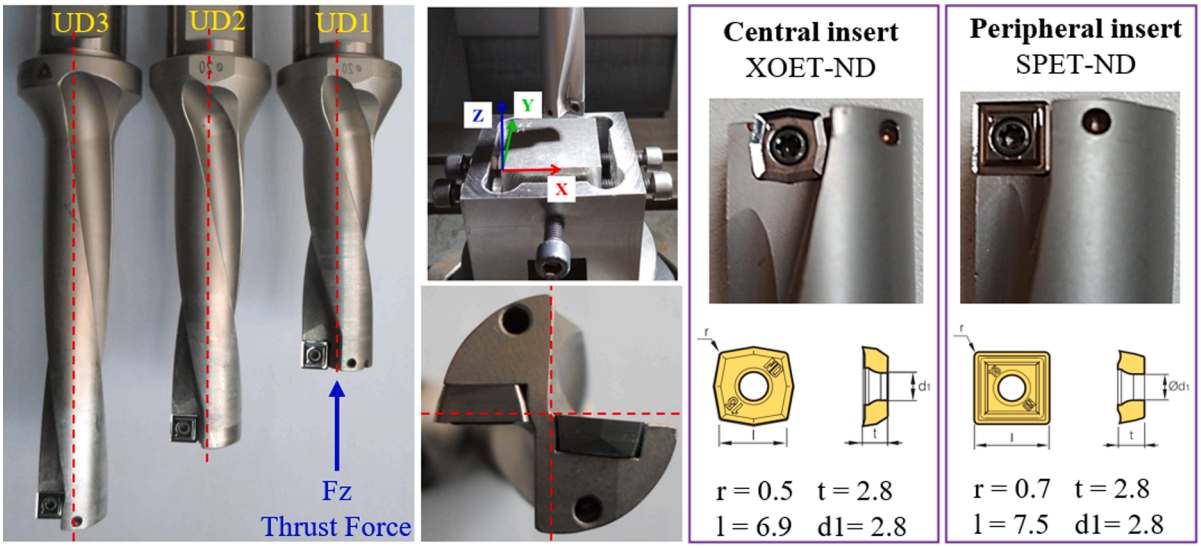


Fig. 4. Used U drills and inserts.

Table 5
Determined features.

Code	Feature's Name
X1	Tensile strength (Mpa)
X2	Yield strength (Mpa)
X3	Elongation (%)
X4	Modulus of elasticity (Gpa)
X5	Thermal conductivity (W/m-K)
X6	Brinell hardness (HB)
X7	Fe (%)
X8	Si (%)
X9	Mn (%)
X10	Cr (%)
X11	Ti (%)
X12	Cu (%)
X13	Mg (%)
X14	Zn (%)
X15	Vc (m/min)
X16	Cutter

2.3.1. Chemical composition

Chemical examinations were performed individually to determine whether the three aluminum alloys utilized were of the desired quality despite being purchased from the manufacturer as certified. The chemical composition determined for each sample was determined by averaging the three measurements made. A Bruker Q4 Tasman model optical emission spectrometer was used for chemical analysis. The device uses arc spark spectrometers. Eight chemical element ratios were analyzed in the chemical composition of materials with aging properties. The analyzed elements are Mg, Cu, Fe, Si, Cr, Zn, Mn, and Ti.

2.3.2. Mechanical properties

By comparing the mechanical attributes of the workpieces with the certificates, it has been determined by the tests whether they are within the desired quality limits. Six mechanical properties were determined. Brinell hardness values were obtained using the Emcotest Duravision 200 universal hardness device. The thermal conductivity was taken from the material database for the respective workpiece alloys. Tensile strength, yield strength, elongation, and elastic modulus were obtained from the tensile test.

2.3.3. Cutter and cutting speed

U drill was used as a cutter for drilling experiments. Although the U drills used have the same nominal diameter, all the bodies have different properties. All of the inserts have identical coatings and geometric properties. The cutting speed was determined as low, medium, and high among the cutting ranges determined in accordance with the selected materials. The feed rate was kept constant in all experiments.

2.4. Pearson correlation coefficient

There are various correlation coefficients, such as Pearson and Spearman. The Pearson approach is employed if the data are normally distributed; otherwise, the Spearman method is utilized [39]. The Pearson correlation coefficient (Pcc) was calculated using equation (7). $\bar{y}_i$ represents the mean of the estimated values.

$$Pcc = \frac{\sum_{i=1}^{n}(t_i - \bar{t}_i)(y_i - \bar{y}_i)}{\sqrt{\sum_{i=1}^{n}(t_i - \bar{t}_i)(y_i - \bar{y}_i)^2}} \quad (7)$$

Since the p-value is >0.05 between the properties determined in this study and the thrust force, the data conform to the normal distribution. As a result, the features were chosen and ranked using the Pearson correlation coefficient algorithm. The extent of the link between characteristics and thrust force is indicated by Pearson correlation coefficients in Fig. 5. The data are sorted according to the absolute values of the calculated coefficients. There is a relationship between the correlation coefficients and the predictive ability of the system [32]. According to this relationship, the correlation coefficient between 0.5 and 0.70 indicates a low forecast for the system, 0.7 to 0.90 indicates a medium prognosis for the system, and greater than 0.9 indicates a high prediction for the system. A negative correlation indicates an inverse relationship between the two variables. According to Fig. 4, none of the individual features have a high correlation with the output response. Therefore, it is desirable to establish models with higher correlations by combining different features. Thus, it is aimed at estimating the thrust force with the least input feature.

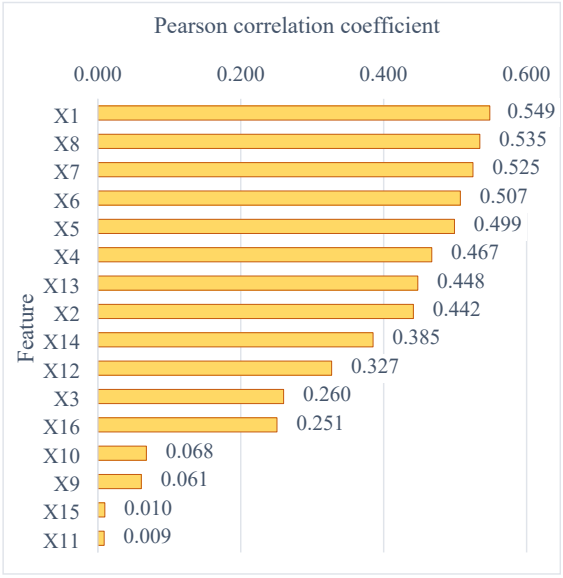


Fig. 5. Relationship between thrust force and properties.

Pearson correlation coefficients were ordered from largest to smallest in order to obtain higher prediction success by combining different features. Datasets were created by adding a new feature each time. The generated datasets were modeled with four single machine learning algorithms and seven hybrid structures and compared with each other with the help of performance evaluation criteria. According to the order shown in Table 6, 16 different feature groups, namely 16 datasets, were created by adding one feature at a time. That is, for the number one data set, a feature with the highest Pearson correlation number was determined as the input, and the estimation of the thrust force was aimed at. The highest two Pearson correlation coefficients for data set number two and all the features for data set number 16 were determined as input, and the thrust force was tried to be estimated with a high success rate.

2.5. Principal component analysis

A statistical technique called principal component analysis (PCA) is used to create new variables that can best account for the variation of multivariate data. PCA can be used to reduce the size of the data, visualize it, filter out noise, or pre-process it for other analyses such as regression [34]. While PCA is used for linear datasets, kernel PCA is used for nonlinear datasets in the literature. The principal component analysis (PCA) method locates linear combinations of the initial features (principal components) that best reflect the variance in the data. When the underlying data relationships are nonlinear, these linear combinations may not effectively capture the important patterns in the data. As a result, PCA may not reduce the dimensionality effectively, and the transformed data may still require a high number of dimensions to explain the variance. Additionally, when PCA is applied to non-linear data, negative effects such as loss of information and misleading interpretation may occur [37]. In this study, PCA was used because there were linear data sets. PCA does not remove correlation between

Table 6
Selected features according to Pearson.

Selection	Number of features selected according to Pearson															Number of features
1	1															1
2	1	8														2
3	1	8	7													3
4	1	8	7	6												4
5	1	8	7	6	5											5
6	1	8	7	6	5	4										6
7	1	8	7	6	5	4	13									7
8	1	8	7	6	5	4	13	2								8
9	1	8	7	6	5	4	13	2	14							9
10	1	8	7	6	5	4	13	2	14	12						10
11	1	8	7	6	5	4	13	2	14	12	3					11
12	1	8	7	6	5	4	13	2	14	12	3	16				12
13	1	8	7	6	5	4	13	2	14	12	3	16	10			13
14	1	8	7	6	5	4	13	2	14	12	3	16	10	9		14
15	1	8	7	6	5	4	13	2	14	12	3	16	10	9	15	15
16	1	8	7	6	5	4	13	2	14	12	3	16	10	9	15	11 16

variables in dataset. The original correlated variables are instead changed into a set of new, uncorrelated variables known as principle components. The linear combinations of the initial variables that make up these principal components represent the majority of the data's volatility. The principal components are brand-new, independently varying variables that increase the variance of the data. The dataset's essence can be captured with minimal information loss if the number of primary components is less than the original size of the data.

A principal component analysis was performed for sixteen features in this study. The four principal components obtained according to the analysis results visualized in Fig. 6 explain approximately 99.9% of the dataset. Thus, 16 features were defined as inputs, and as a result, four principal components were determined and taken into account. For the four principal components resulting from the examination, models were established with all machine learning algorithms and compared with each other and with 16 other data sets.

3. Experimental results and discussion

This study's objective is to predict thrust force using machine learning algorithms with minimum input data and a high success rate in indexable drilling of aluminum materials. Unlike other studies in the literature, chemical composition, mechanical properties, and drilling parameters were introduced as inputs to the model, and for the purpose of estimating the thrust force, machine learning methods were utilized. Other research estimate cutting parameters by using features taken from various signal information in the time or frequency domain received throughout the experiment, such as cutting speed, feed rate, or features [34]. However, processing the signal from the accumulated data takes a lot of time and expertise. Results cannot be generalized for each different material class. However, with the proposed method, the feature matrix can be easily created and does not require expertise. The certificate obtained from the supply firm lists a material's chemical and mechanical characteristics, and information may also be found in a number of material databases. Thus, even though they have never been included in the dataset, it aims to estimate the thrust force by entering the chemical composition and mechanical characteristics of other material groups that belong to the same class. For the proposed method, eight chemical compositions and six mechanical properties were determined, taking into account the common elements found in aluminum-class alloys. In addition, cutting speed and U drill data are included in the input dataset as input parameters. Chemical composition ratios were measured by optical emission spectrometry. The elements determined as input properties by measurement are Fe, Ti, Si, Cu, Mn, Mg, Cr, and Zn. By mixing these elements in different proportions, different series of aging aluminum alloys are produced. For example, the major alloying element other than Al in the 2xxx series aluminum alloys is Cu; for the 6xxx series, it is Mg-Si; and for the 7xxx series, it is Mg-Zn. The mechanical properties of all the alloys obtained are different from each other. Within the scope of this study, mechanical properties were obtained using tensile tests, hardness tests, and material databases. Yield strength, tensile strength, elongation, and elastic modulus were obtained from the tensile test. While the brinell hardness value was obtained with the hardness test, thermal conductivities were taken from the material database. Within the scope of this study, the mechanical properties determined as input properties are the features used to compare many different alloys and understand their machinability. Three cutting speeds and three U drill types were also determined as input features. Data sets were obtained using all these features. The datasets, which were created with a total of sixteen features, were used for the

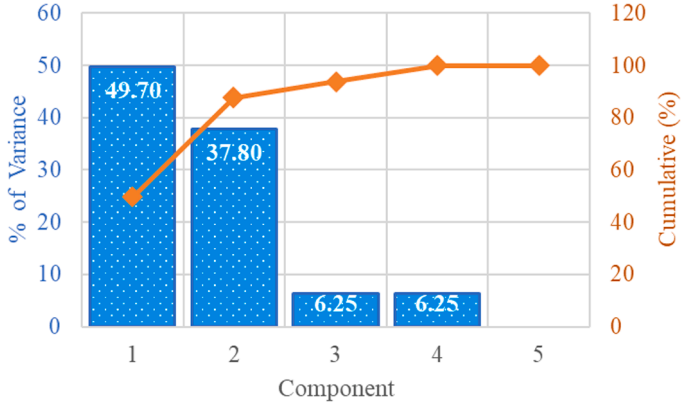


Fig. 6. Principal component analysis and contribution ratios of components.

estimation of the thrust force by modeling with machine learning algorithms. A total of 17 datasets were used for the highly successful estimation of thrust force in indexable drilling. Regression algorithms were used because the input features and output responses consisted of quantitative data. The chemical composition and mechanical properties were checked with test devices to confirm the information written in the workpiece material certificate received from the material supplier. The obtained data were compared and examined. It has been determined that the data is compatible.

The relationship between the determined properties and the thrust force is given in Fig. 7. Chemical composition changes the properties of a material. Although the chemical composition remains unchanged, different heat treatments can alter the material's mechanical qualities, such as hardness [29]. The change in mechanical properties has a great influence on the output responses, such as the thrust force that occurs in hole-making. Consequently, it is essential to consider both mechanical and chemical qualities simultaneously. When the Figure is examined, the thrust force values decreased in parallel with the increase in the tensile strength, yield strength, and hardness values. Because the built-up edge and smeared material in aluminum alloys cause adhesion between the insert and the body, resulting in increased forces [40]. However, with the increase in mechanical property values, chip breakability increased [41]; therefore, material smearing decreased, resulting in a degradation in thrust force. The thrust force rose along with the chemical structure's Si ratio. The cutting speed variation was not very effective for the specified cutter and aluminum alloys. With the increase in Mg and Zn ratios, the thrust force values decreased. It has been established in the literature that adding Cu and Zn to an aluminum alloy makes it harder and reduces thrust force [42]. Increases and decreases occur for certain size ranges of chemical composition or mechanical properties. The microstructure and secondary phases within it were not considered in this study. As a result, drilling parameters and input features have an effect on the thrust force. Some features have less impact, and some have a higher impact. For example, cutting speed changes on thrust force vary less, while cutter type is quite significant and varies more. The input properties determined for mechanical properties and chemical composition all affect the thrust force and cause different forces to be obtained. Thrust force is very important as it is closely related to torque, temperature, and hole quality.

Fig. 8 shows the Pearson correlation table between mechanical properties and chemical composition. This table was created based on the information obtained from materials A2, A6, and A7. Chemical elements in the structure of a material and some mechanical properties have high positive and negative correlations. For example, yield

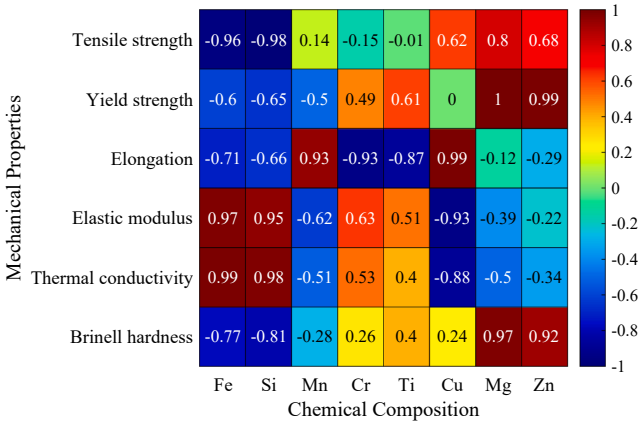


Fig. 8. Pearson correlation table between mechanical properties and chemical composition.

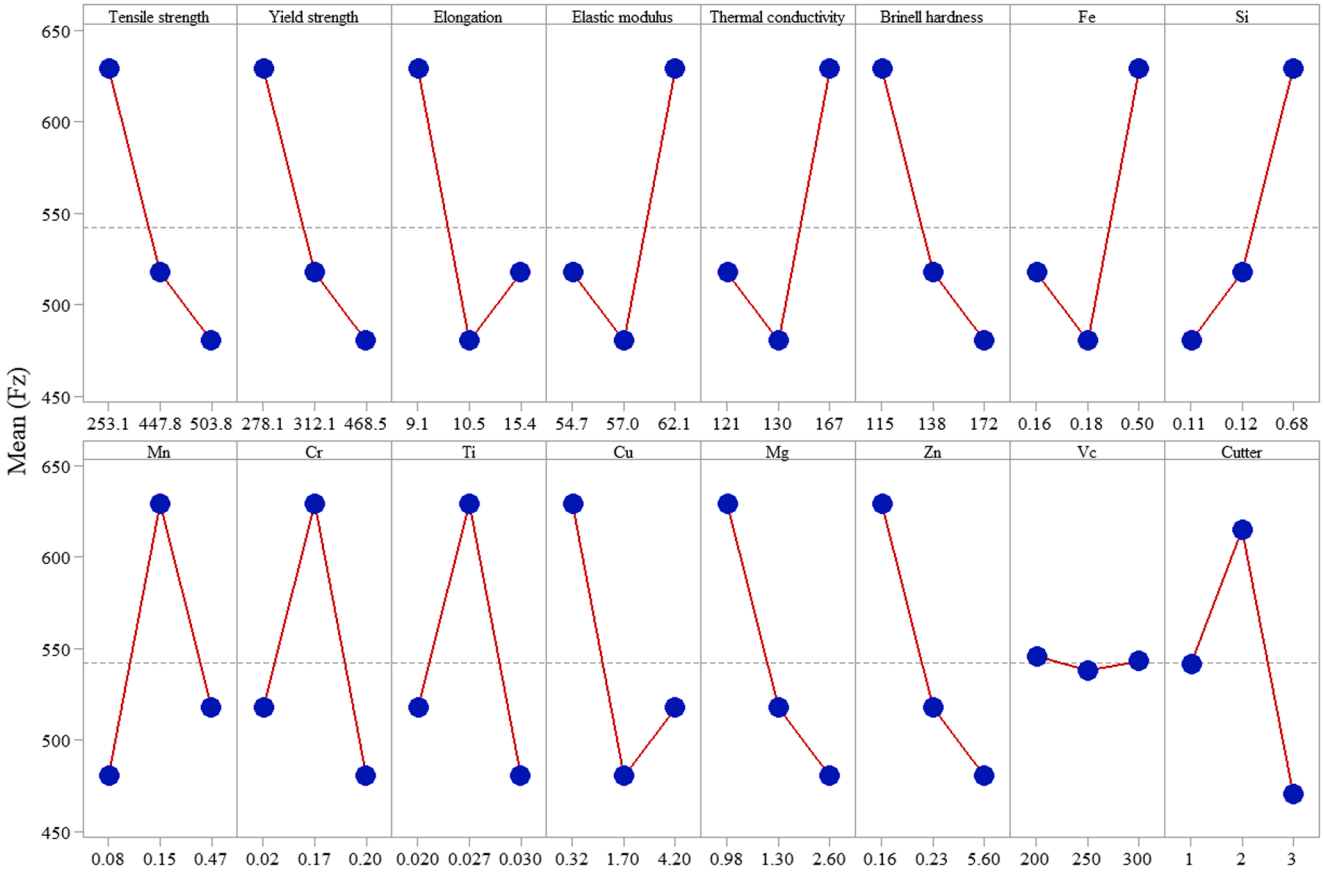


Fig. 7. Main effect plot of thrust force with determined properties.

strength has a highly positive correlation with Mg and Zn elements. A good correlation indicates that the traits change together as a whole. Fe and Si elements have a strong negative association with tensile strength. Negative correlation means that there is an inverse relationship between features. As one increases, the other decreases, or as one decreases, the other increases.

In this study, four single machine learning algorithms, including XGBoost, GPR, SVM, and FFNN, were determined for modeling and prediction purposes. These algorithms are preferred because of their short computation time and high prediction success. In addition, seven hybrid structures were obtained in order to increase the prediction success of these four algorithms and make them more balanced. A more powerful and efficient model can be created using hybrid structures and a combination of different machine learning techniques that are related to or complement each other [43]. Overfitting problems can be eliminated by making higher generalizations [44]. Various research in the literature have employed comparable hybrid architectures. Six performance evaluation metrics, including MAD, MSE, RMSE, MAPE, SE, and R^2, were used to compare the outcomes from the established models.

In order to make the closest estimation to the experimental result with the least input of data for chemical composition, mechanical properties, and drilling parameters, all properties were ordered from largest to smallest according to the Pearson correlation coefficient. A total of 16 datasets were created by adding one feature at a time. In addition, principal component analysis and dimensionality reduction have been applied to successfully estimate the thrust force with minimum features. As a result of the data reduction, four features were calculated and compared with all single and hybrid machine learning structures. Table 7 provides the comparison findings of the models according to the test datasets. As seen in the table, the model with the most successful coefficient of determination belongs to the XGBoost-FFNN hybrid structure expressed with the symbol HM4. Compared to single machine learning algorithms, the hybrid model showed better prediction success. Single-model FFNN also showed good prediction performance with a lower MAPE value. However, when compared to the other 16 datasets, the coefficient of determination was low and the RMSE value was high. In other words, it can be said that while less estimation errors are made on average with FFNN compared to the XGBoost-FFNN hybrid structure, the size of the errors made is large.

In Table 8, sixteen datasets were created with the features listed according to the Pearson correlation coefficient, and the dataset with four features obtained by PCA was compared with the help of the established models. The closer the coefficient of determination is to 1, the higher the prediction success of the model is considered. While the PCA dataset determination coefficient was 0.9938 with the HM4 model, the dataset with nine features gave a higher value of 0.9952. Among the models established for the 17 datasets compared in the table, the models with the highest coefficient of determination were obtained with both single and hybrid models. Considering the coefficient of determination, the SM1 model for 8 of 17 datasets, the HM2 model for 3, the HM3 model for 2, the HM4 model for 3, and finally the HM5 model for 1 gave the highest value. The highest coefficient of determination could not be obtained for any dataset for the single models SM2, SM3, and SM4, and for the hybrid models HM1, HM6, and HM7. The highest coefficient of determination of 0.9972 for all established models and datasets was obtained with the SM1 model and the dataset of 13 feature numbers. The lowest coefficient of determination was 0.9339, calculated with the SM3 model for the four features calculated with PCA. While hybrid structures performed better for models established with a dataset with a lower number of variables, the superiority of the FFNN model was clearly revealed as the number of characteristics increased. However, for the 15 features there are, the HM3 model also resulted in a higher coefficient of determination. Considering the determination coefficients, all the models created gave successful results in the estimation of the thrust force. Another striking point is that when the dataset with 16 features and the dataset determination coefficients created by reducing the dataset to 4 features with PCA are compared, very close results are obtained. However, for feature number 2, the HM5 model determination coefficient was 0.9963. This value is better than the coefficient of determination of 0.9938 obtained by PCA. Creating models by identifying features with a high correlation with Pearson is as effective as PCA feature reduction. While the coefficient of determination for SVM was found to be 0.89 in a study, improvement was achieved by obtaining a value of 0.99 with the SVM performed after PCA [45]. However, such a development did not occur in the present study. There was a slight decrease in the coefficient of determination after PCA.

The violin plot is obtained in Fig. 9 according to the determination coefficients calculated by the models established for all datasets. For all datasets, the smallest data range distribution was obtained with the SM1 model, while the highest data distribution range was obtained with the SM3 model. According to the table and Figure, the FFNN model is less affected by the number of features, while the XGBoost, GPR, and SVM models are more affected, respectively.

The graphical comparison of the models established for the datasets created according to the number of features is visualized in Fig. 10 according to the MAPE and R^2 values. The highest R^2 values were obtained with the datasets with features 2, 9, 13, and 14. For the determined alloys belonging to the aluminum material class, two properties were entered, and the thrust force was estimated with high success. While some established models have more successful prediction abilities, others have relatively less success. In some established models, with an increase in the number of input variables, the MAPE value increases and the R^2 value deteriorates significantly. Determining machine learning algorithms according to the number of dataset features is important for establishing optimal models. These optimum models are possible by using and comparing more than one machine learning algorithm.

Some comparisons were made to examine higher-performing datasets and models in more detail. For these comparisons, performance evaluation criteria were calculated with SM1, SM4, HM1, HM2, HM4, and HM5 models for the number of features 2, 9, 13, and 14 with

Table 7
Performance comparison for four principal components.

PCA for the four principal components		Performance criteria					
Symbol	**Models**	**MAD**	**MSE**	**RMSE**	**MAPE**	**SH**	**R^2**
SM1	FFNN	37.88	2172.39	46.61	6.88	53.82	0.9925
SM2	GPR	93.37	15843.70	125.87	22.40	145.34	0.9455
SM3	SVM	100.67	19236.19	138.69	24.21	160.15	0.9339
SM4	XGBoost	58.43	4818.00	69.41	11.05	80.15	0.9834
HM1	GPR + FFNN	52.14	4274.87	65.38	12.46	75.50	0.9853
HM2	GPR + SVM	95.82	17431.20	132.03	23.07	152.45	0.9401
HM3	SVM + FFNN	60.38	5344.88	73.11	14.21	84.42	0.9816
HM4	XGBoost + FFNN	40.17	1816.63	42.62	7.81	49.22	**0.9938**
HM5	XGBoost + GPR	63.88	7302.05	85.45	14.02	98.67	0.9749
HM6	XGBoost + SVM	73.66	8548.73	92.46	16.05	106.76	0.9706
HM7	XGBoost + GPR + SVM + FFNN	62.13	5920.81	76.95	14.11	88.85	0.9797

Bold value = Highest coefficient of determination.

Table 8
Comparison of the coefficients of determination of the established models.

R^2	Established models										
Datasets	**SM1**	**SM2**	**SM3**	**SM4**	**HM1**	**HM2**	**HM3**	**HM4**	**HM5**	**HM6**	**HM7**
1	**0.9838**	0.9541	0.9518	0.9551	0.9732	0.9535	0.9736	0.9755	0.9553	0.9536	0.9656
2	0.9912	0.9932	0.9858	0.9925	0.9956	0.9952	0.9889	0.9919	**0.9963**	0.9896	0.9940
3	0.9890	0.9922	0.9904	0.9899	0.9926	**0.9935**	0.9898	0.9895	0.9928	0.9903	0.9920
4	0.9925	0.9924	0.9913	0.9905	0.9933	**0.9934**	0.9922	0.9916	0.9923	0.9914	0.9927
5	0.9920	0.9801	0.9914	0.9919	0.9878	0.9880	0.9917	**0.9924**	0.9879	0.9923	0.9906
6	0.9927	0.9921	0.9929	0.9919	0.9935	**0.9940**	0.9931	0.9923	0.9930	0.9929	0.9935
7	0.9922	0.9742	0.9909	0.9912	0.9874	0.9847	**0.9923**	0.9917	0.9858	0.9916	0.9898
8	**0.9905**	0.9831	0.9844	0.9879	0.9882	0.9849	0.9888	0.9894	0.9863	0.9870	0.9879
9	0.9951	0.9711	0.9918	0.9951	0.9874	0.9851	0.9937	**0.9952**	0.9873	0.9939	0.9915
10	**0.9909**	0.9777	0.9802	0.9888	0.9862	0.9803	0.9864	0.9899	0.9850	0.9849	0.9860
11	**0.9924**	0.9821	0.9912	0.9920	0.9894	0.9890	0.9921	0.9923	0.9890	0.9921	0.9912
12	**0.9947**	0.9811	0.9519	0.9724	0.9916	0.9829	0.9895	0.9880	0.9782	0.9888	0.9923
13	**0.9972**	0.9671	0.9761	0.9964	0.9898	0.9731	0.9928	0.9969	0.9893	0.9929	0.9916
14	**0.9956**	0.9446	0.9531	0.9953	0.9871	0.9505	0.9886	0.9954	0.9872	0.9886	0.9883
15	0.9848	0.9553	0.9619	0.9713	0.9828	0.9626	**0.9872**	0.9801	0.9792	0.9812	0.9841
16	**0.9941**	0.9535	0.9559	0.9920	0.9928	0.9560	0.9929	0.9940	0.9891	0.9899	0.9917
PCA	0.9925	0.9455	0.9339	0.9834	0.9853	0.9401	0.9816	**0.9938**	0.9749	0.9706	0.9797

Bold value: The highest coefficients of determination of the datasets.

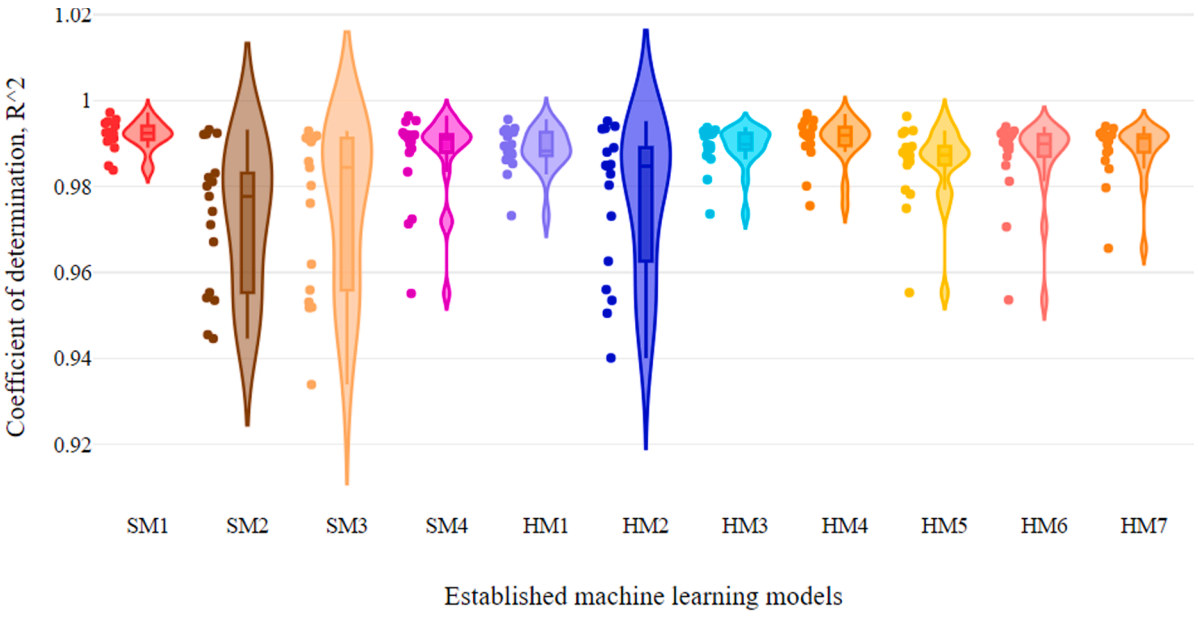


Fig. 9. Distribution of the coefficients of determination calculated by the established models.

determination coefficients higher than 0.995. Calculated performance values are compared in Tables 9–12.

Table 9 shows that high estimation success can be achieved for the dataset created with two features. According to the table, the highest performance predictions were obtained with hybrid models. The GPR method has been used in many studies due to its high success rate in estimation. For feature number 2, hybrid models GPR + FFNN, GPR + SVM, and GPR + XGBoost showed superior performance. MAPE values resulted in less than 5. The machine learning algorithms mentioned alone could not pass the determination coefficient of 0.995. However, they produced remarkably high coefficients of determination in other established models. In a study in the literature, MAPE and R^2 values were calculated as 5.12/0.98 for GPR, 7.91/0.97 for SVM, and 10.85/0.95 for ANN, respectively, as a result of modeling the cutting forces generated by turning AISI 4340 material [25]. In another study, SVM was calculated as 5.31/0.995 and ANN 8.87/0.98 in drilling copper material with HSS, while SVM was calculated as 5.25/0.97 and ANN 7.13/0.96 for cast iron material [36]. In another study, GPR (0.91), SVM (0.88), and ANN (0.91) models were compared with R^2 values, respectively [27]. The success of established hybrid models is obvious when compared with the literature.

For feature number 2, the model obtained with GPR gave a successful result. However, when Table 10 is examined, the models obtained with FFNN and XGBoost performed more successfully for feature number 9. The XGBoost + FFNN hybrid model also produced successful performance values. In the same way, successful performance values were obtained with the models established with the same machine learning algorithms in Tables 11 and 12. Another point that draws attention from the tables is that the MAPE values increase as the number of feature selections increases. Lower MAPE values were obtained with lower feature selection numbers. In a study, specific cutting energy and surface roughness were modeled with XGboost, and MAPE values were calculated as 6.94 and 6.64, respectively [46]. Compared with the literature, the success of the performance values obtained from the models established for the current study is obvious.

The models for feature selection numbers 2, 9, 13, and 14 are graphically compared in Fig. 11. Bar charts were used to compare different data sets in the tables and to better visualize the trends. Some

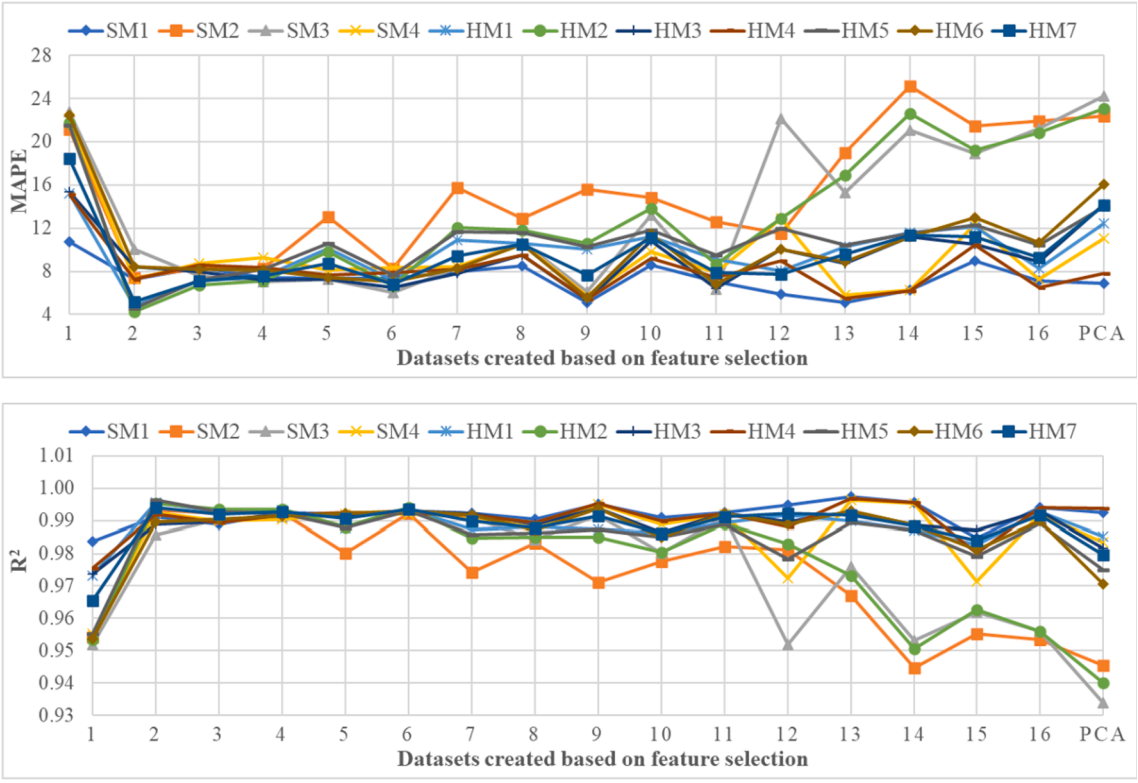


Fig. 10. Graphical comparison of performance for all datasets.

Table 9
Comparison of performance according to feature selection number 2.

Number of feature selections = 2		Performance criteria					
Symbol	**Models**	**MAD**	**MSE**	**RMSE**	**MAPE**	**SE**	**R^2**
SM1	FFNN	42.94	3155.85	56.18	7.30	64.87	0.9912
SM2	GPR	45.15	2444.81	49.44	7.46	57.09	0.9932
SM3	SVM	60.25	5080.41	71.28	10.08	82.30	0.9858
SM4	Xgboost	42.78	2674.55	51.72	7.28	59.72	0.9925
HM1	GPR + FFNN	27.99	1568.19	39.60	4.78	45.73	**0.9956**
HM2	GPR + SVM	25.23	1707.77	41.33	4.30	47.72	**0.9952**
HM3	SVM + FFNN	50.48	3996.09	63.21	8.46	72.99	0.9889
HM4	XGBoost + FFNN	42.86	2898.57	53.84	7.29	62.17	0.9919
HM5	XGBoost + GPR	26.84	1325.01	36.40	4.60	42.03	**0.9963**
HM6	XGBoost + SVM	50.40	3724.95	61.03	8.45	70.47	0.9896
HM7	XGBoost + GPR + SVM + FFNN	30.38	2135.69	46.21	5.22	53.36	0.9940

Bold value: The highest coefficients of determination.

Table 10
Comparison of performance according to feature selection number 9.

Number of feature selections = 9		Performance criteria					
Symbol	**Models**	**MAD**	**MSE**	**RMSE**	**MAPE**	**SE**	**R^2**
SM1	FFNN	30.96	1728.48	41.57	5.11	48.01	**0.9951**
SM2	GPR	94.00	10199.66	100.99	15.57	116.62	0.9711
SM3	SVM	38.12	2907.49	53.92	6.15	62.26	0.9918
SM4	Xgboost	33.26	1719.52	41.47	5.70	47.88	**0.9951**
HM1	GPR + FFNN	60.71	4437.71	66.62	10.05	76.92	0.9874
HM2	GPR + SVM	64.56	5257.14	72.51	10.55	83.72	0.9851
HM3	SVM + FFNN	33.04	2231.29	47.24	5.32	54.54	0.9937
HM4	XGBoost + FFNN	32.11	1703.76	41.28	5.41	47.66	**0.9952**
HM5	XGBoost + GPR	61.67	4473.18	66.88	10.31	77.23	0.9873
HM6	XGBoost + SVM	34.19	2159.97	46.48	5.62	53.67	0.9939
HM7	XGBoost + GPR + SVM + FFNN	46.47	2996.37	54.74	7.67	63.21	0.9915

Bold value: The highest coefficients of determination.

Table 11
Comparison of performance according to feature selection number 13.

Number of feature selections = 13		Performance criteria					
Symbol	**Models**	**MAD**	**MSE**	**RMSE**	**MAPE**	**SE**	**R^2**
SM1	FFNN	25.41	814.09	28.53	5.11	32.95	**0.9972**
SM2	GPR	78.20	9721.13	98.60	18.99	113.85	0.9671
SM3	SVM	67.04	7050.42	83.97	15.30	96.96	0.9761
SM4	Xgboost	28.49	1055.86	32.49	5.84	37.52	**0.9964**
HM1	GPR + FFNN	41.42	3016.31	54.92	10.29	63.42	0.9898
HM2	GPR + SVM	71.03	7934.84	89.08	16.88	102.86	0.9731
HM3	SVM + FFNN	37.75	2134.48	46.20	8.76	53.35	0.9928
HM4	XGBoost + FFNN	26.95	903.11	30.05	5.47	34.70	**0.9969**
HM5	XGBoost + GPR	41.65	3165.73	56.26	10.41	64.97	0.9893
HM6	XGBoost + SVM	37.99	2099.08	45.82	8.88	52.90	0.9929
HM7	XGBoost + GPR + SVM + FFNN	39.70	2483.20	49.83	9.59	57.54	0.9916

Bold value: The highest coefficients of determination.

Table 12
Comparison of performance according to feature selection number 14.

Number of feature selections = 14		Performance criteria					
Symbol	**Models**	**MAD**	**MSE**	**RMSE**	**MAPE**	**SE**	**R^2**
SM1	FFNN	30.06	1214.96	34.86	6.24	40.25	**0.9956**
SM2	GPR	97.13	15157.74	123.12	25.17	142.16	0.9446
SM3	SVM	79.43	12826.68	113.25	21.08	130.78	0.9531
SM4	Xgboost	30.15	1291.69	35.94	6.26	41.50	**0.9953**
HM1	GPR + FFNN	44.31	3521.04	59.34	11.59	68.52	0.9871
HM2	GPR + SVM	85.51	13542.33	116.37	22.62	134.37	0.9505
HM3	SVM + FFNN	44.27	3118.09	55.84	11.24	64.48	0.9886
HM4	XGBoost + FFNN	29.92	1248.86	35.34	6.22	40.81	**0.9954**
HM5	XGBoost + GPR	43.90	3501.16	59.17	11.53	68.32	0.9872
HM6	XGBoost + SVM	43.87	3114.40	55.81	11.18	64.44	0.9886
HM7	XGBoost + GPR + SVM + FFNN	44.09	3200.09	56.57	11.38	65.32	0.9883

Bold value: The highest coefficients of determination.

datasets and some models performed relatively poorly, while others performed better. Linear trendlines have been added to the charts. The amount of MAPE obtained tends to increase more with a rise in the quantity of characteristics, especially when taking into account the shape and trend lines for the MAPE value. There is a tendency to achieve higher performance with fewer features.

The comparison of actual and anticipated responses for test datasets of the best models is shown in Fig. 12. In general, strong and accurate predictions were made. While the actual test data and the forecast data were in agreement, some data showed a lower agreement.

Which data set and model performed better was determined by considering the performance evaluation criteria. It is assumed that the model with a higher coefficient of determination and a lower MAPE value performs better. In summary, when comparing the performance of models for datasets obtained through principal component analysis and the Pearson correlation coefficient, the model with at least 2 features and HM5 demonstrated a remarkably high determination coefficient of 0.9963. The XGBoost + GPR hybrid model was the model that showed high performance with the least input data. The FFNN, XGBoost, and XGBoost + FFNN models showed the best performance for feature numbers 9, 13, and 14. As can be seen from the graphs obtained, the MAPE value tended to increase as the number of features in the datasets increased. With a minimum of two features entered in accordance with chemical composition, mechanical properties, and drilling settings, it has been discovered that the thrust force may be predicted with a high degree of success using machine learning algorithms. For the prediction of thrust force in indexable drilling of aluminum alloys, the MAPE and coefficient of determination of hardened (aged) aluminum alloys were calculated as 4.89/0.996 for A2, 4.94/0.997 for A6, and 9.31/0.99 for A7, respectively. The obtained values show the success of the established models.

4. Conclusion

Determining the thrust force is important in terms of output variables such as power consumption, tool wear, and surface roughness. The thrust force was gauged with a dynamometer. The measurement of thrust force with a dynamometer can only be made under experimental conditions. Extra clamping tools are required for clamping workpieces to the dynamometer. The dynamometer is a rather expensive and sensitive instrument. Once the data is received, time and expert knowledge are required to process the data and make inferences. This is not suitable for every part in a real production environment. In the literature, various approaches have been suggested as remedies for this issue. Among these methods used for U drills, the solutions produced by FEA, mathematical, and mechanistic approaches are controversial, and a clear solution could not be produced. Modeling with Taguchi, ANN, and ANFIS does not take into account the mechanical and chemical properties of different workpieces. Alternately, new techniques based on machine learning are required for calculating thrust force.

The objective of this work is to forecast the thrust force that occurs when drilling aluminum alloys with a U drill by identifying the minimum number of input features using machine learning methods. As a result of the investigation, the thrust force may be calculated using the two aluminum-class attributes with a very high estimation success rate. These properties are tensile strength from mechanical properties and Si ratio from chemical composition. The proposed method has many benefits. These include reducing the measuring cost, saving time, eliminating the extra clamping tools and dynamometer costs, shortening the machine setup time, efficient planning of the process, etc. In this study, the thrust force occurring in the replaceable drilling of aluminum alloys, which is a gap in the literature, was successfully predicted by machine learning algorithms. In addition, unlike other studies, models were successfully created by considering the chemical compositions and

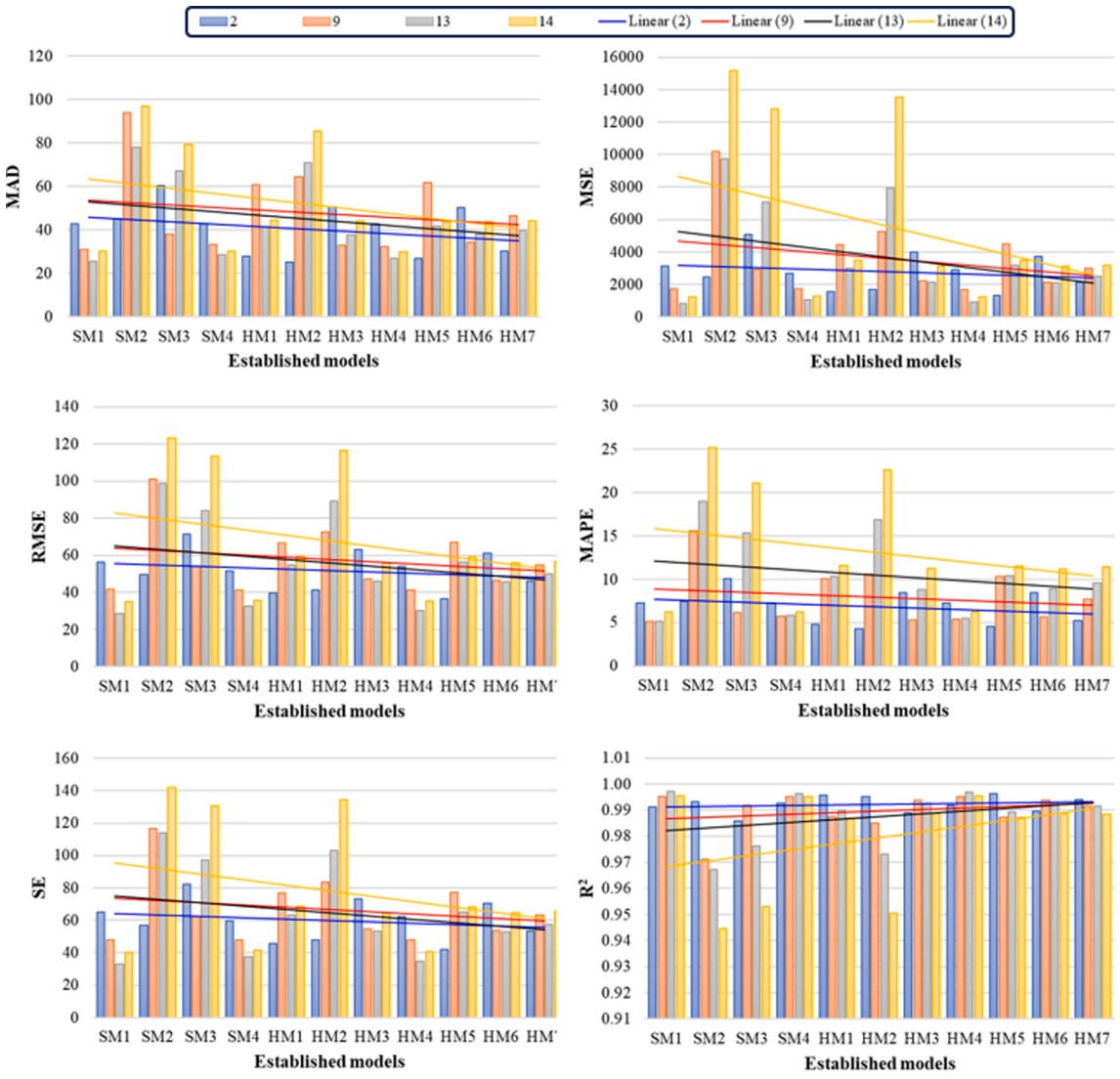


Fig. 11. Graphical comparison of models for higher performing datasets.

mechanical properties of the workpiece materials as inputs in the estimation of the thrust force. It may be claimed that FFNN models perform better as the number of attributes in the datasets rises, but hybrid models perform better when there are fewer features in the datasets. According to the performance evaluation criteria, the estimation inaccuracy grows as the variety of characteristics increases. A higher coefficient of determination was calculated for the GPR + FFNN, GPR + SVM, and GPR + XGBoost hybrid constructs established separately with GPR for the two feature numbers. The MAPE values obtained are less than 5. Better performing models for feature numbers 9, 13, and 14 were FFNN, XGBoost, and FFNN + XGBoost. The success of the models created based on the dataset's feature count has varied. However, the determination coefficients for all of the established models were within acceptable limits. To sum up, the thrust force can be successfully predicted by machine learning algorithms by entering two properties, including tensile strength and Si ratio, when drilling aluminum-class aging alloys with a U drill.

5. Future works

This study has been prepared for the estimation of the thrust force using machine learning algorithms and minimum input properties in drilling aluminum materials with U drills. The scope of this study can be expanded with more data. Future work can be listed as follows:

- Data can be collected for material classes other than aluminum, such as steel, stainless steel, and cast iron.
- Models can be built with different machine learning algorithms and hybrid structures.
- Different feature selection and sorting algorithms can be preferred.
- Models can be built for output responses such as surface roughness, power consumption, and tool wear.

CRediT authorship contribution statement

Aslan Akdulum: Visualization, Conceptualization, Methodology, Validation, Resources. **Yunus Kayir:** Methodology, Supervision, Formal analysis.

Declaration of competing interest

The authors declare that they have no known competing financial interests or personal relationships that could have appeared to influence the work reported in this paper.

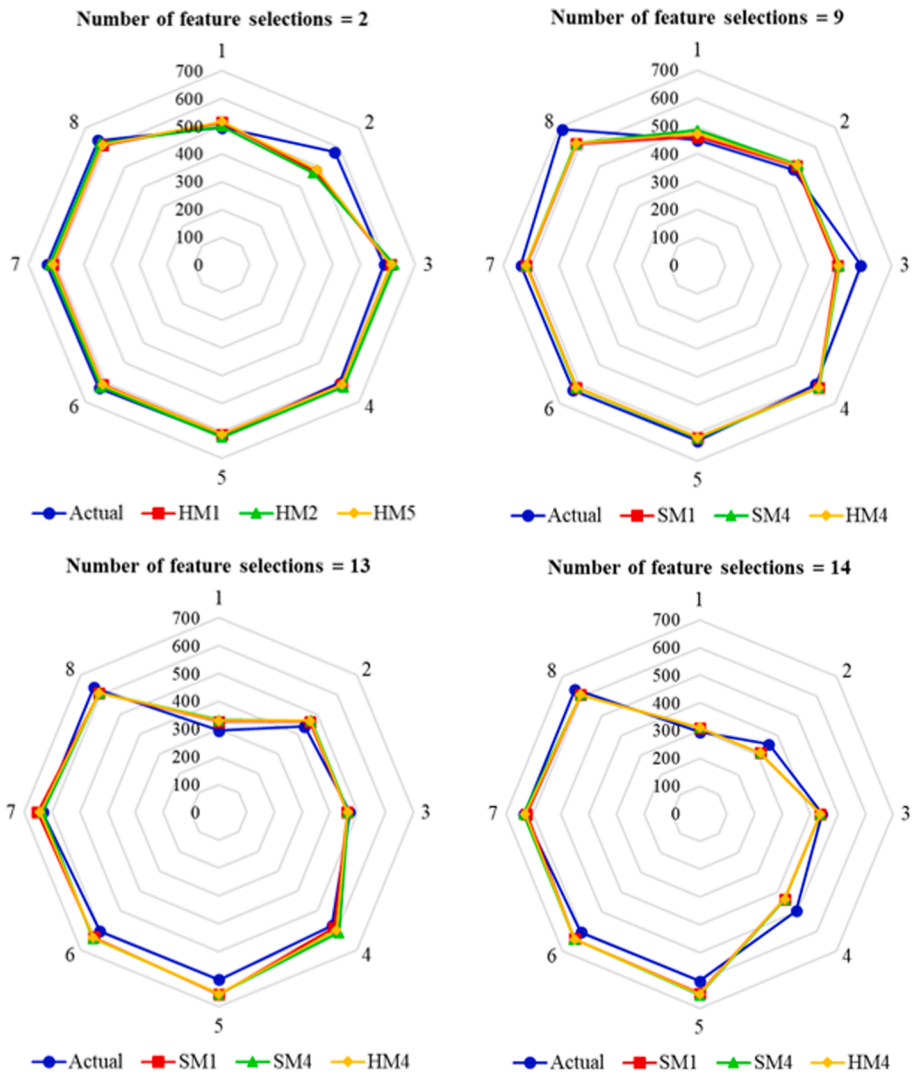


Fig. 12. Comparison of test datasets.

Data availability

Data will be made available on request.

Acknowledgements

It was supported by grant number 07/2019-08 from the Gazi University's Scientific Research Projects Unit. The researchers acknowledge the help of the BAP department at Gazi University.

References

[1] N. Yaşar, Thrust force modelling and surface roughness optimization in drilling of AA-7075: FEM and GRA, J. Mech. Sci. Technol. 33 (10) (2019) 4771–4781, https://doi.org/10.1007/s12206-019-0918-5.
[2] M.C. Santos, et al., Machining of aluminum alloys: a review, Int. J. Adv. Manuf. Technol. 86 (2016) 3067–3080, https://doi.org/10.1007/s00170-016-8431-9.
[3] B. Dhakal, S. Swaroop, Effect of laser shock peening on mechanical and microstructural aspects of 6061–T6 aluminum alloy, J. Mater. Process. Technol. 282 (2020), 116640, https://doi.org/10.1016/j.jmatprotec.2020.116640.
[4] L. Troeger, E. Starke Jr, Microstructural and mechanical characterization of a superplastic 6xxx aluminum alloy, Mater. Sci. Eng. A 277 (1–2) (2000) 102–113, https://doi.org/10.1016/S0921-5093(99)00543-2.
[5] R.A. Gonçalves, M.B. da Silva, É.S. Costa, Statistical analysis of cutting forces and hole accuracy in reaming an Al–Si–Mg alloy (6351) with different copper contents, J. Braz. Soc. Mech. Sci. Eng. 40 (2018) 1–19, https://doi.org/10.1007/s40430-018-1450-8.
[6] V.P. Astakhov, Drills: science and technology of advanced operations, CRC Press, 2014.
[7] A. Akdulum, Y. Kayır, Investigation of the effect of u drills with different properties on thrust force, torque and spindle load, Politeknik Dergisi 26 (1) (2023) 387–400, https://doi.org/10.2339/politeknik.1113301.
[8] A. Parsian, Regenerative Chatter Vibration in Indexable Drills: Modeling and Simulation, University West, 2018.
[9] M. Günay, T. Meral, Modelling and multiresponse optimization for minimizing burr height, thrust force and surface roughness in drilling of ferritic stainless steel, Sādhanā 45 (1) (2020) 273, https://doi.org/10.1007/s12046-020-01490-3.
[10] H. Kim, et al., Real-time drill wear estimation based on spindle motor power, J. Mater. Process. Technol. 124 (3) (2002) 267–273, https://doi.org/10.1016/S0924-0136(02)00111-5.
[11] S. Kim, Integration of pre-simulation and sensorless monitoring for smart mould machining, Int. J. Simul. Modell. 15 (4) (2016) 623–636, https://doi.org/10.2507/IJSIMM15(4)4.354.
[12] K. Patra, et al., Artificial neural network based tool condition monitoring in micro mechanical peck drilling using thrust force signals, Precis. Eng. 48 (2017) 279–291, https://doi.org/10.1016/j.precisioneng.2016.12.011.
[13] Z. Kilic, Y. Altintas, Generalized mechanics and dynamics of metal cutting operations for unified simulations, Int. J. Mach. Tool Manuf. 104 (2016) 1–13, https://doi.org/10.1016/j.ijmachtools.2016.01.006.
[14] L.L. Liu, L.P. Zhou, Z.J. Ying, The FEM Dynamic Simulation in the Drilling process with Indexable Inserts, in: Advanced Materials Research. 2012. Trans Tech Publ.10.4028/www.scientific.net/AMR.557-559.1292.
[15] A. Kheireddine, et al., An FEM analysis with experimental validation to study the hardness of in-process cryogenically cooled drilled holes in Mg AZ31b, Procedia Cirp 8 (2013) 588–593, https://doi.org/10.1016/j.procir.2013.06.156.
[16] D. Svensson, T. Andersson, A. Andersson Lassila, Coupled Eulerian-Lagrangian simulation and experimental investigation of indexable drilling, Int. J. Adv. Manuf. Technol. (2022).

[17] M. Kaymakci, Z. Kilic, Y. Altintas, Unified cutting force model for turning, boring, drilling and milling operations, Int J Mach Tool Manu 54 (2012) 34–45, https://doi.org/10.1016/j.ijmachtools.2011.12.008.
[18] A. Parsian, et al., A mechanistic approach to model cutting forces in drilling with indexable inserts, Procedia Cirp 24 (2014) 74–79, https://doi.org/10.1016/j.procir.2014.07.138.
[19] A. Akdulum, Y. Kayir, Modeling and estimation of thrust force, torque, and surface roughness in indexable drilling of AA6061-T651 with Taguchi, ANN, and ANFIS, Sādhanā 48 (3) (2023) 143, https://doi.org/10.1007/s12046-023-02209-w.
[20] A. Akdulum, Y. Kayir, Experimental investigation and optimization of process stability in drilling of Al 7075–T651 using indexable insert drills, J. Braz. Soc. Mech. Sci. Eng. 45 (8) (2023) 429, https://doi.org/10.1007/s40430-023-04303-w.
[21] M. Rahman, K. Seah, V. Venkatesh, Performance evaluation of endrills, Int J Mach Tool Manu 28 (4) (1988) 341–349, https://doi.org/10.1016/0890-6955(88)90048-X.
[22] C. Jochem, Mechanics and dynamics of drilling, Ph. D. Thesis, Faculty of Applied Science, University British Columbia, 2006.
[23] V. Venkatesh, W. Xue, A study of the built-up edge in drilling with indexable coated carbide inserts, J. Mater. Process. Technol. 58 (4) (1996) 379–384, https://doi.org/10.1016/0924-0136(95)02211-2.
[24] Y. Zhang, X. Xu, Predicting thrust force during drilling of composite laminates with step drills through the Gaussian process regression, Multidiscipline Model. Mater. Struct. 18 (5) (2022) 845–855, https://doi.org/10.1108/MMMS-07-2022-0123.
[25] M.S. Alajmi, A.M. Almeshal, Modeling of cutting force in the turning of AISI 4340 using Gaussian process regression algorithm, Appl. Sci. 11 (9) (2021) 4055, https://doi.org/10.3390/app11094055.
[26] C. Liu, et al., Predicting residual properties of ball screw raceway in whirling milling based on machine learning, Measurement 173 (2021), 108605, https://doi.org/10.1016/j.measurement.2020.108605.
[27] M. Cheng, et al., Prediction of surface residual stress in end milling with Gaussian process regression, Measurement 178 (2021), 109333, https://doi.org/10.1016/j.measurement.2021.109333.
[28] N. Guo, et al., Analysis and prediction of the influence of milling parameters on CFRP strength based on XGBoost algorithm, J. Braz. Soc. Mech. Sci. Eng. 45 (7) (2023) 346, https://doi.org/10.1007/s40430-023-04267-x.
[29] R. Rashad, T. El-Hossainy, Machinability of 7116 structural aluminum alloy, Mater. Manuf. Process. 21 (1) (2006) 23–27, https://doi.org/10.1080/AMP-200060603.
[30] A.R. Froehlich, et al., The correlation of machinability and microstrutural characteristics of different extruded aluminum alloys, J. Mater. Eng. Perform. 16 (2007) 784–791, https://doi.org/10.1007/s11665-007-9097-0.
[31] J. Zander, R. Sandström, Modelling technological properties of commercial wrought aluminium alloys, Mater. Des. 30 (9) (2009) 3752–3759, https://doi.org/10.1016/j.matdes.2009.02.004.
[32] M.K. Uçar, et al., Estimation of body fat percentage using hybrid machine learning algorithms, Measurement 167 (2021), 108173, https://doi.org/10.1016/j.measurement.2020.108173.
[33] Q. Lu, et al., Combination of thermodynamic knowledge and multilayer feedforward neural networks for accurate prediction of MS temperature in steels, Mater. Des. 192 (2020), 108696, https://doi.org/10.1016/j.matdes.2020.108696.
[34] H. Zhou, et al., Multi-condition wear prediction and assessment of milling cutters based on linear discriminant analysis and ensemble methods, Measurement 216 (2023), 112900, https://doi.org/10.1016/j.measurement.2023.112900.
[35] T. Chen, C. Guestrin, Xgboost: A scalable tree boosting system, in: Proceedings of the 22nd acm sigkdd international conference on knowledge discovery and data mining, 2016. 10.48550/arXiv.1603.02754.
[36] M.S. Alajmi, A.M. Almeshal, Predicting the tool wear of a drilling process using novel machine learning XGBoost-SDA, Materials 13 (21) (2020) 4952, https://doi.org/10.3390/ma13214952.
[37] D. Kong, Y. Chen, N. Li, Gaussian process regression for tool wear prediction, Mech. Syst. Sig. Process. 104 (2018) 556–574, https://doi.org/10.1016/j.ymssp.2017.11.021.
[38] M. Vogt, V. Kecman, Active-set methods for support vector machines, in: Support Vector Machines: Theory and Applications, Springer, 2005, pp. 133–158.
[39] M.K. Uçar, et al., The effect of training and testing process on machine learning in biomedical datasets, Mathematical Problems in Engineering, 2020, 2020. 10.1155/2020/2836236.
[40] P. Mueller-Hummel, Process understanding of dry drilling CFRP/aluminium and AL/AL stacks in IT8 quality, SAE Int. J. Aerosp. 9 (2016–01-2116) (2016).
[41] P.A.B. Machado, et al., Investigation on machinability in turning of as-cast and T6 heat-treated Al-(3, 7, 12%) Si-0.6% Mg alloys, J. Manuf. Process. 75 (2022).
[42] Ş. Bayraktar, F. Afyon, Machinability properties of Al–7Si, Al–7Si–4Zn and Al–7Si–4Zn–3Cu alloys, J. Braz. Soc. Mech. Sci. Eng. 42 (2020) 1–12, https://doi.org/10.1007/s40430-020-02281-x.
[43] G. Xu, X. Wang, Support vector regression optimized by black widow optimization algorithm combining with feature selection by MARS for mining blast vibration prediction, Measurement (2023) 113106, https://doi.org/10.1016/j.measurement.2023.113106.
[44] B. Li, et al., Non-invasive milling force monitoring through spindle vibration with LSTM and DNN in CNC machine tools, Measurement 210 (2023), 112554, https://doi.org/10.1016/j.measurement.2023.112554.
[45] W. Zhang, et al., An experimental modeling of cyclone separator efficiency with PCA-PSO-SVR algorithm, Powder Technol. 347 (2019) 114–124, https://doi.org/10.1016/j.powtec.2019.01.070.
[46] J. Zhang, et al., Research on feasible region of specific cutting energy and surface roughness in high-speed dry milling of 30CrMnSiNi2A steel with CVD and PVD coated inserts, Int. J. Adv. Manuf. Technol. 125 (1–2) (2023) 133–155, https://doi.org/10.1007/s00170-022-10647-9.